Am J Cancer Res 2022;12(2):574-584
www.ajcr.us /ISSN:2156-6976/ajcr0139618

Original Article

Multimodality imaging in the assessment of bone marrow-derived mesenchymal stem cell therapy for doxorubicin-induced cardiomyopathy

Chanjuan Qu[1], Jian Wang[1], Yuqing Wang[2], Fangfei He[3], Xudong Shi[4], Zhuoli Zhang[5], Yining Wang[1]

[1]Department of Radiology, State Key Laboratory of Complex Severe and Rare Diseases, Peking Union Medical College Hospital, Chinese Academy of Medical Sciences and Peking Union Medical College, Beijing 100730, China; [2]Tsinghua Laboratory of Brain and Intelligence, Tsinghua University, Beijing 100084, China; [3]National Center for Nanoscience and Technology (NCNST), Beijing 100190, China; [4]Key Laboratory of Human Disease Comparative Medicine, National Health Commission of China (NHC), Institute of Laboratory Animal Sciences, Peking Union Medicine College, Chinese Academy of Medical Sciences, Beijing 100021, China; [5]Radiology & Biomedical Engineering Chao Family Comprehensive Cancer, University of California, Irvine, USA

Received October 6, 2021; Accepted December 22, 2021; Epub February 15, 2022; Published February 28, 2022

Abstract: Due to their broad-spectrum effects and high antitumor efficacies, anthracycline-based chemotherapies are commonly prescribed in various solid and hematological malignancies. Doxorubicin (DOX) is one of the most highly used anthracyclines but has been shown to cause lethal cardiomyopathy in clinical practice. Studies have demonstrated that bone marrow-derived mesenchymal stem cells (BMSCs) have the ability to rescue DOX-induced cardiomyopathy (DIC). However, novel molecular imaging techniques are required to explore the biological behaviors, safety, eventual viability, and environmental interactions of transplanted stem cells during therapy. To investigate the biological behaviors of transplanted BMSCs, we applied bioluminescence imaging (BLI) and magnetic resonance imaging (MRI) techniques to trace firefly luciferase (Fluc) and ultrasmall superparamagnetic iron oxide (USPIO) double-labeled mouse BMSCs after injection into the heart apex in a chronic DIC mouse model. Then, we determined the optimal BMSC number for transplantation into the heart and optimized MRI parameters to evaluate transplanted BMSCs *in vitro* and *in vivo*. Our results showed that the BLI trace signal could last 7 days in the DIC mouse model, whereas the MRI signal lasted up to 3 days. However, MRI provided more detailed pathophysiological information on DIC than BLI, such as inflammation and fibrosis signs. The optimal *in vivo* cell number for BLI and MRI was determined to be 1×10^6. In conclusion, BLI combined with multimodality MRI could be used to monitor the biological behavior of BMSCs transplanted into a chronic DIC mouse model in a visual and dynamic manner.

Keywords: Bone marrow-derived mesenchymal stem cells, bioluminescence imaging, magnetic resonance imaging, doxorubicin-induced cardiomyopathy, multimodality imaging

Introduction

Doxorubicin (DOX) as one of the Anthracyclines, is widely used to treat solid tumors and hematological malignancies based on their broad spectrum and high antitumor efficacy [1, 2]. However, dose-dependent cardiotoxicities, such as lethal cardiac insufficiency and cardiac failure, limit the use of DOX [1-6]. Thirty percent of DOX-treated childhood cancer patients have been found to suffer from heart failure upon the long-term follow-up of adult survivors [7]. DOX can cause acute and chronic myocardial toxicity. Acute DOX-induced cardiotoxicity (DIC) is easily detected, and the prognosis is good upon DOX withdrawal. However, more attention should be given to chronic DIC, which is irreversible, and no efficient therapies are currently available to reverse cardiac fibrosis or cardiac cavity enlargement and lower the heart ejection fraction changes related to lethal chronic heart failure. DOX-induced heart failure is commonly progressive and irreversible, with a predicted 2-year survival rate of 40% [8].

The primary purpose of stem cell therapy is to repair tissues with functional cells differentiated from stem cells and for stem cells to improve

the lost organ function together with residual functional native cells [9, 10]. Stem cells have the abilities of self-renewal, proliferation, and multidirectional differentiation, which have been confirmed to be lacked in the adult. Whether other source-derived stem cells can slow cardiomyocyte necrosis and apoptosis, reduce fibrosis and increase the heart ejection fraction remains to be clarified [11]. Recently, different types of stem cells have been used to treat cardiovascular diseases, such as myocardial infarction and ischemia-reperfusion injury [12-15]. The mechanisms of stem cell repair in myocardial injury mainly include stem cell differentiation into cardiomyocytes or promotion of new blood vessel formation and irreversible secretion of cardioprotective factors through paracrine pathways to regulate cell differentiation and local inflammation [16-23]. However, whether stem cells can be successfully transplanted remains to be determined. Moreover, the eventual survival, biological behaviors, safety, differentiation ability, interactions with the environment and mechanisms of transplanted stem cells *in vivo* are unclear, which limits the clinical application of stem cell therapy. Therefore, novel molecular imaging techniques for *in vivo* tracing and visualization of the biological behaviors of stem cells after transplantation are urgently needed [24-27].

Due to their low immunogenicity, ability to differentiate into various cells, tissues and organs, and ability to serve as rich sources, we herein investigated the efficacy of bone marrow-derived mesenchymal stem cells (BMSCs) to improve chronic DIC, dilated cardiomyopathy and heart insufficiency as well as their biological behaviors after transplantation into the heart. With aim to investigate the constantly ongoing biological behavior and process of transplanted BMSCs *in vivo* in chronic DIC or heart failure mouse model, safe, noninvasive and real-time monitoring imaging modality should be developed and employed. However, each imaging method has its own unique advantages and disadvantages based on their imaging mechanism. Our study chose to adopt BLI combined with MRI multimodality imaging to fulfill the purpose. Bioluminescence imaging (BLI) is based on the detection of light generated by the enzyme luciferase catalyzed oxidation reaction of a substrate luciferin. In vivo BLI is a noninvasive way to measure light output from luciferase-expressing cells after luciferin administration in living organisms. Compared with fluorescence imaging (FI), BLI has relatively higher sensitivity and specificity, with much higher signal-to-noise ratio, which could detect at least 10^2 luciferase expressing cells at a deeper location in the organism. Several recent reports have transplanted the transfected luciferase expressing cells into the targeted location to detect the biological behavior of organism. Both FI and BLI has relatively low tissue permeability, otherwise, D-luciferin has a heterogeneous biodistribution in the body [28, 29]. Meanwhile, MRI techniques have high spatial resolution and soft tissue resolution so that it could offer detailed message involving the anatomy and function of heart. However, MRI has low sensitivity, and are limited by motion effects associated with the cardiac cycle and diaphragmatic movements when utilized for cardiac imaging. Therefore, multiple imaging modality including BLI and MRI were combined in our study to clarify the mechanisms of transplanted BMSCs treatment in chronic DIC. Furthermore, the ability of BMSCs from Balb/c mice to prevent immune rejection was tested by transplanting BMSCs into the hearts of Balb/c mice with chronic DIC. BLI combined with multimodality MRI was found to monitor the biological behavior of BMSCs transplanted into a chronic DIC mouse model in a visual and dynamic manner.

Materials and methods

Reagents

DMEM, trypsin-EDTA and fetal bovine serum (FBS) were obtained from Gibco (Grand Island, USA). Cell counting kit-8 reagents were purchased from Beyotime.

Institute of Biotechnology (Shanghai, China). DOX was obtained from Innochem (Peiking, China). Vivotrax was obtained from Magnetic Insight Inc. (Alameda, USA). D-luciferin and potassium salt were obtained from Gold Biotechnology (Gold Biotechnology, St. Louis, Missouri).

Isolation, purification and identification of BMSCs from Balb/c mice

All animal studies were performed according to the protocol approved by the Peking Union

Medical College Hospital (Beijing, China) Animal Care and Use Committee. After being sacrificed by CO_2 administration followed by cervical dislocation, newborn mice (Balb/c, 1-2 days old) were soaked in 75% alcohol for 5 minutes, and then, the bilateral hind legs were dislocated from the body. The femurs and tibias were transferred into low-glucose DMEM with 1% PS after careful removal of the muscles attached to the bones. The bone marrow was flushed into a 50 ml centrifuge tube on ice as follows: both ends of the tibias and femurs were cut off, a 26-gauge needle attached to a 5 ml syringe with precooled complete medium was inserted into the bone marrow cavity, and washing was repeated until the bones turned white. After centrifugation at 1500 rpm for 5 minutes, the supernatant was discarded; the cell pellets were resuspended in complete low-glucose DMEM medium, seeded in a petri dish (a 60 mm petri dish for one mouse) and routinely incubated overnight in a 37°C cell incubator with 5% CO_2.

The supernatant was discarded, and the cells were washed twice with sterile PBS to remove the nonadherent cells. The attached cells were cultured with fresh culture medium supplemented every two days, and the cell morphology was observed.

Stable expression of the Fluc reporter gene (Fluc-BMSCs) in BMSCs from Balb/c mice and bioluminescence imaging in vitro

The Fluc reporter gene was expressed in BMSCs (Fluc-BMSCs) by lentiviral transfection. Undifferentiated Fluc-BMSCs that had been passaged 4-6 times were used. Bioluminescence imaging (BLI) of the Fluc-BMSCs was performed according to the manufacturer's instructions. Briefly, 200 μl of Fluc-BMSCs were seeded in each well of a 96-well flat-bottom plate at different concentrations (1×10^6, 5×10^5, 2.5×10^5, 1×10^5, 5×10^4, and 2.5×10^4). After 150 μg/ml D-luciferin was added to each well, a series of bioluminescence images were acquired successively with 60-second exposure times until the BLI signal was attenuated.

Cell culture and cytotoxicity studies

Mouse BMSCs were maintained in DMEM supplemented with 10% FBS in an incubator containing 5% CO_2 under 95% humidity. BMSCs plated in 96-well plates at a density of 1×10^4/well were cultured for 12 h before being challenged with Vivotrax dissolved in serum-free DMEM at various final concentrations (0-100 μg/ml) for different times (4, 12, 24 or 48 h), and then 10 μl of CCK-8 solution was added to each well. The absorbance at 450 nm was measured using a POLARstar OPTIMA multidetection microplate reader after a 2-h incubation at 37°C.

A series of working dilutions of DOX in serum-free DMEM were prepared. H9C2 cells plated in 96-well plates at a density of 5×10^3 per well were cultured for 24 h before being challenged with various concentrations of DOX (0-10 μM) in DMEM for 12 h, and then, 10 μl of CCK-8 solution was added to each well. After incubation at 37°C for 2 h, the absorbance at 450 nm was measured using a POLARstar OPTIMA multidetection microplate reader.

Labeling of Fluc-BMSCs with USPIO particles (Fluc/USPIO-BMSCs) and magnetic resonance imaging (MRI) in vitro

Fluc-BMSCs were seeded in cell culture flasks with labeling media containing USPIO (Vivotrax 80 μg/ml) and incubated at 37°C in 5% CO_2. Prussian blue staining was used to investigate the distribution of iron particles in the cells.

Chronic doxorubicin-induced cardiomyopathy mouse model establishment and BMSC transplantation

BALB/c mice aged 6-8 weeks were purchased from Beijing HFK Bioscience Co., Ltd. and received intraperitoneal injection of 2 mg/kg DOX 6 times weekly to induce cardiac fibrosis formation after 3 months. Fluc/USPIO-BMSCs were then suspended in PBS at a concentration of 1×10^6/ml. Fluc/USPIO-BMSCs (50 μl) were injected into the left ventricular apical area of Balb/c mice after the mice had been anesthetized with intraperitoneal injection of 10% chloral hydrate (0.03 mg/kg).

BLI of Balb/c model mice in vivo

The *in vivo* BLI was acquired on day 1 after Fluc/USPIO-BMSC injection using the Night-OWL LB 983 *in vivo* imaging system (IVIS). Briefly, D-luciferin dissolved in saline was injected intraperitoneally into the mice anes-

thetized by isoflurane inhalation at a dose of 150 mg/kg body weight. Five minutes after the injection, a series of bioluminescence images were acquired at 5-min acquisition intervals for approximately 30 min until the luciferin was washed out. The image with the peak BLI intensity was quantified in units of photon counts.

BLI and MRI of Fluc/USPIO-BMSCs in Balb/c mice

Balb/c mice were randomly divided into an experimental group (n=20) and a control group (n=10). All mice were subjected to the same experimental procedures, except for mice in the experimental group that received treatment with Fluc/USPIO-BMSCs.

BLI of both groups was performed on day 1, day 3, day 5 and day 7 after injection, according to the imaging schedule previously mentioned.

Since the MRI signal lasts for up to 3 days and the characteristic MRI signal becomes visually undetectable at day 4, MRI of both groups was performed on day 1 and day 3 with T2, T2*, and gradient recalled echo (GRE) cine sequence on an Inova 7.0-T magnetic resonance scanner (Varian) [24]. The electrocardiography, respiration, and core temperature of mice were monitored using an MRI-compatible system (SA Instruments) after the mice were anesthetized with 1.5% isoflurane in 1 L/min oxygen. Ten cardiac phases were acquired for each cine series, which were triggered by the electrocardiogram.

Images from successive slices along the short cardiac axis were then acquired with a slice thickness of 1 mm. Five slices were typically required to cover the left ventricle from the apex to the base. Hypointense areas in the myocardium were evaluated to trace the implanted cells. Other MRI parameters included the following: FOV, 30×30 mm; matrix, 200×200; FA, 30; TR, 100 ms; NEX, 5.0; and TE, 6.0 ms.

Histological analysis

Mice in the BMSC-treated group were euthanized after the BLI signal disappeared. The heart tissues were fixed in 4% paraformaldehyde and embedded in paraffin, and the 5-μm-thick sections were stained with hematoxylin-eosin (H&E)s. Images of the stained sections were obtained using a light microscope (Nikon Eclipse TE2000-U, Japan) at 200× magnification.

Statistical analysis

Data for continuous variables that conformed to a normal distribution are presented as the mean ± standard deviation. Statistical analysis was performed with GraphPad Prism 5.0 software. Comparisons between the two independent groups were performed using Student's *t*-test. Two-sided tests were used throughout the experiments. $P<0.05$ was considered statistically significant. Multiple group comparisons were performed by one-way analysis of variance (ANOVA) followed by the least significant difference (LSD) *t*-test for post hoc analysis.

Results

The Fluc reporter gene was stably expressed by lentiviral infection in BMSCs derived from Balb/c mice

BMSCs from Balb/c mice were primarily round mononuclear cells. After 4 to 12 h, BMSCs with a spindle shape were attached to the bottom of culture flasks. BMSCs were purified by passing the cells to passage 4. Then, the 4th passage cells were cultured in Balb/c mouse MSC osteogenic differentiation medium (Cyagen Biosciences) for 2 weeks, and the formed calcium nodules were then stained using alizarin red (**Figure 1A**). The results indicated that BMSCs with differentiation ability were successfully purified from Balb/c mice.

As shown in **Figure 1B**, the Fluc reporter gene was stably expressed by infection with lentivirus carrying the luciferase reporter gene in BMSCs derived from Balb/c mice.

Cytotoxic evaluation of Vivotrax

As displayed in **Figure 1C**, the viability of Balb/c BMSCs incubated with 100 μg/ml Vivotrax for 4 h was significantly different compared with that of BMSCs in the control group. The viability was significantly different between the 80-100 μg/ml group and the control group after incubation with Vivotrax for 12 h. As the Vivotrax incubation time increased, the toxicity of Vivotrax

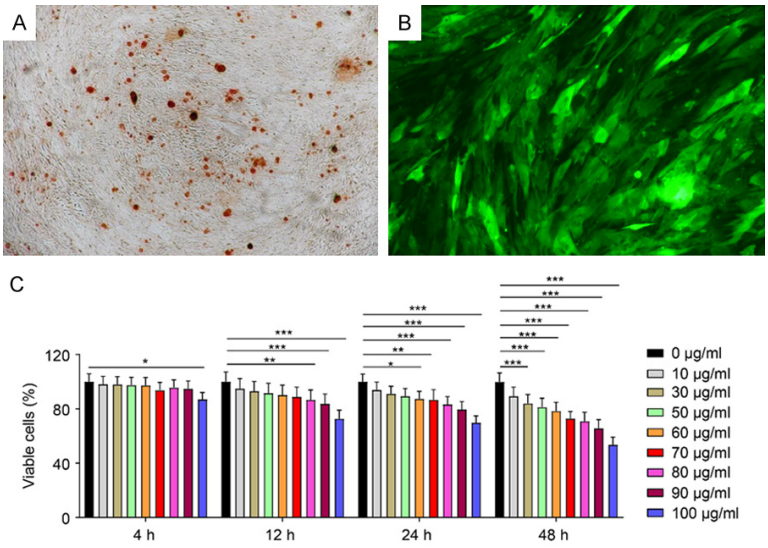

Figure 1. A. Alizarin red staining indicating osteogenesis of Balb/c mouse-derived BMSCs. B. Balb/c BMSCs labeled with GFP-LUC. C. CCK-8 and Vivotrax assessment.

increased. As such, we decided to incubate the cells for 4 h at a concentration of 80 μg/ml.

The chronic DOX-induced cardiomyopathy mouse model was successfully established

H&E staining, PSR staining, and echocardiogram analysis were performed three months after the Balb/c mice received weekly intraperitoneal injections of 2 mg/kg DOX 6 times, and the analyses showed collagen formation (**Figure 2A**). Picric acid-Sirius scarlet staining (**Figure 2B**) and Masson staining (**Figure 2C**) both confirmed the successful generation of a chronic cardiotoxicity Balb/c mouse model, which showed connective tissue formed around the myocardial tissues and blood vessels and increased and thickened collagen fibers in the myocardial interstitium. Cardiac ultrasound (**Figure 2D** and **2E**) showed an enlarged left ventricular cavity and decreased ejection fraction. Taken together, these results indicated the successful establishment of cardiac fibrosis in Balb/c mice.

The viability of the BMSCs was slightly affected by USPIO and FLUC labeling

Distinctive blue cytoplasmic inclusions were clustered in the Fluc-USPIO BMSCs as determined by Prussian blue staining, which demonstrated the successful entrance of USPIO into the cells. The average labeling efficiency was 95-98%. Upon microscopic examination, the Fluc-USPIO BMSCs appeared as spindle-shaped cells with a single nucleus.

The viability of the BMSCs, BMSC-LUC, BMSC-USPIO, and BMSC/LUC-USPIO was determined by CCK-8 assay kits based on the OD values. As shown in **Figure 3A**, there was no significant differences among the BMSCs, BMSC-LUC, BMSC-USPIO, and BMSC/LUC-USPIO at 24 h, suggesting the safety of USPIO and FLUC labeling. Moreover, the viability of the Flu/USPIO-BMSCs was time-dependently decreased in comparison with that of the BMSCs after incubation with USPIO or FLUC, indicating that the cell viability and proliferation ability of BMSCs were slightly affected by USPIO and FLUC labeling. H9C2 cells pretreated with DOX were incubated with normal medium and BMSC medium, and as displayed in **Figure 3B**, the cells incubated with BMSC medium showed significantly higher viability, indicating that BMSCs may have the ability to improve the damaged myocardium through paracrine signals.

Correlations between cell number and BLI intensity and T2 and T2 relaxome values*

As is shown in **Figure 3C**, the photo counts measured by Ivis were linearly correlated with the cell number as follows: y=1766.4x+20492 (R^2=0.9422). A negative correlation between the number of cells and the T2 relaxome value was observed (R^2=0.4680) (**Figure 3D**). The T2* relaxome value measured by MRI was also linearly correlated with the cell number: y=-18.27x+239.5 (R^2=0.9342) (**Figure 3E**). Fluorescence signal and magnetic resonance signal decrease with the decrease of cell number, indicating that double-labeled stem cells can be tracked quantitatively.

BLI signal intensity was gradually decreased to an undetectable level after dual-labeled cell transplantation in vivo

Eighteen mice in the BMSC-treated group and 10 mice in the control group survived DOX administration and intramyocardial injection of

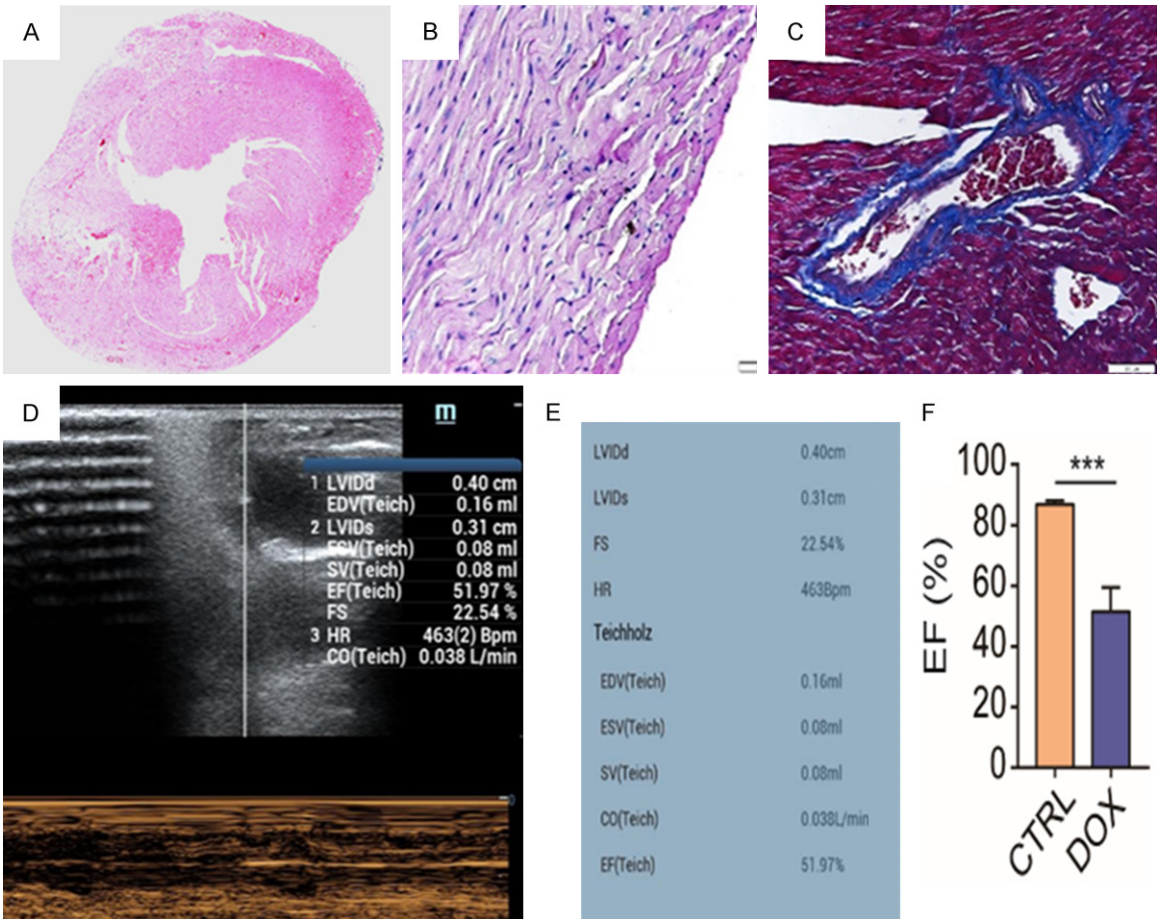

Figure 2. Chronic DOX-induced cardiomyopathy mouse model. A. H&E staining showed connective tissue formation around myocardial tissues and blood vessels and collagen fibers in the myocardial interstitium. B. PSR staining showed increased and thickened collagen fibers (red). C. Masson staining showed collagen fibers (blue). D and E. Cardiac ultrasound showed an enlarged left ventricular cavity and decreased ejection fraction. F. The EF value between CTRL group (healthy mouse) and DOX group (chronic DIC mouse) showed a significant difference.

BMSC/LUC-USPIO. A BLI signal intensity of 1,040,000±1,107,488 counts on day 1 after surgery was detected in the heart region in the BMSC-treated group but decreased to 221,000±159,578.4 on day 3 and 67,700± 106,890.5 on day 5. The signal was beyond the threshold of detection on day 7 in all mice of the experimental group, as shown in **Figure 4**.

The outcome of MRI stem cell tracing was consistent with that of BLI

Corresponding with the injection sites, the signal of the anterior wall (white arrow) of the left ventricle was decreased significantly (**Figure 5A** and **5B**). These hypointense regions were not found in the control group on day 1. Visualization of BMSC/LUC-USPIO stem cells by MRI confirmed their successful intramyocardial delivery and survival, which was in agreement with the results of BLI stem cell tracing.

Histological results

As displayed in **Figure 5C**, Prussian blue staining revealed positive cells with blue USPIO particles, which also proved the successful intramyocardial injection of BMSCs/LUC-USPIO.

Discussion

In the current study, we labeled Fluc-expressing mouse BMSCs with USPIO particles and applied two molecular imaging techniques (BLI and MRI) to monitor the biological behaviors of the transplanted BMSCs in vivo in a chronic DIC mouse model.

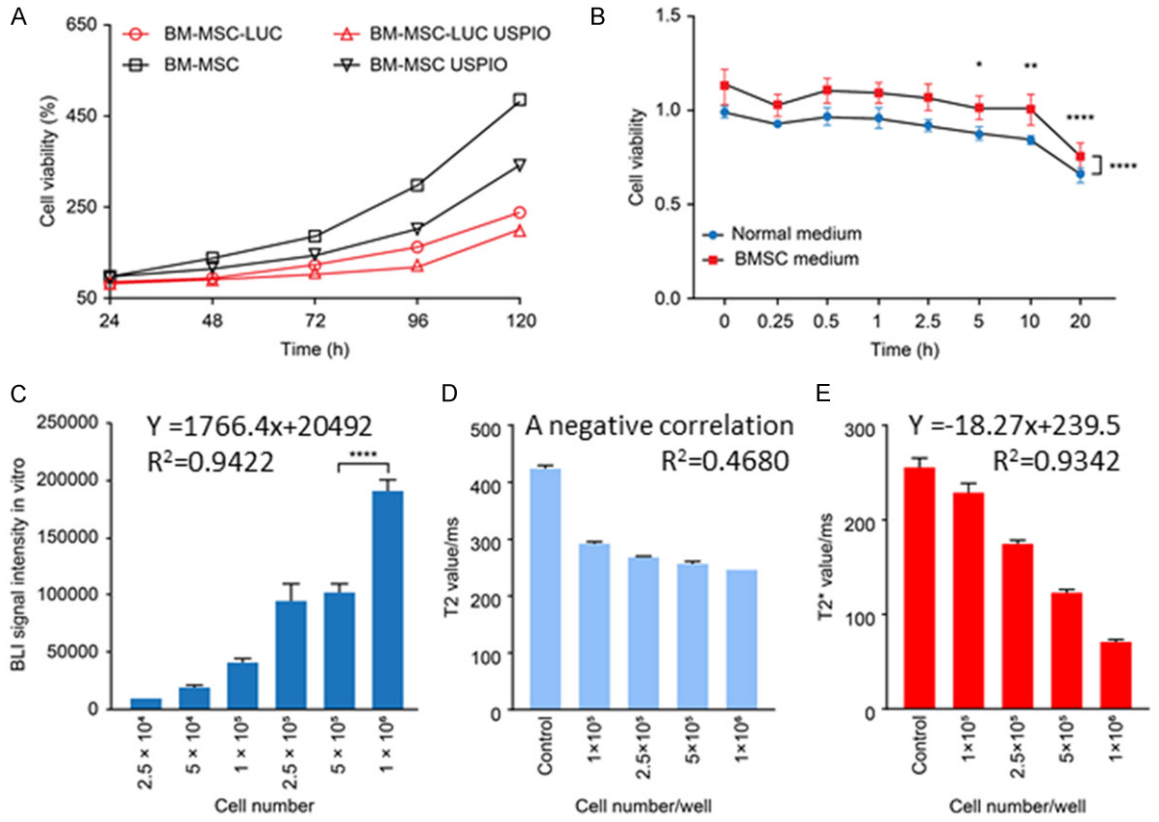

Figure 3. Correlations between cell number and BLI intensity. A. Viability of BMSCs, BMSC-LUC, BMSC-USPIO, and BMSC/LUC-USPIO. B. Viability of H9C2 cells incubated with normal medium and BMSC medium. C. BLI signal *in vitro*. D. T2 value *in vitro*. E. T2* relaxome value *in vitro*.

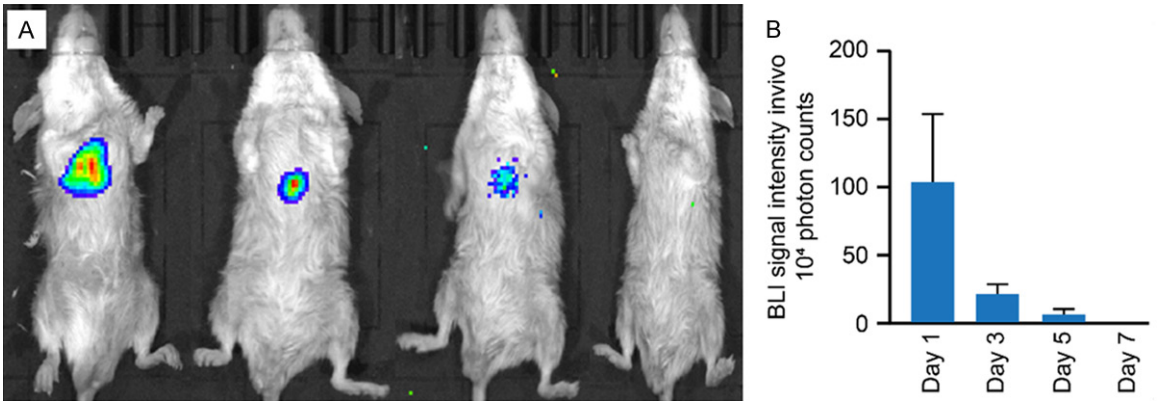

Figure 4. BLI signal intensity *in vivo*. (A) Images of BLI signal intensity. (B) Quantification of the BLI signal intensity in (A).

Mesenchymal stem cells have the abilities of self-renewal, proliferation, and differentiation into multiple cell types, and tissues formed from their own stem cells do not suffer immune rejection. Therefore, stem cells have started to be used in the treatment of many disorders, such as myocardial infarction, kidney damage, liver damage, intestinal disease, skin diseases, and neurological diseases [9, 10]. Brusko et al. [30] highlighted stem cell transplantation in the treatment of diabetes. Because the loss of myocardial fibers or cells and FF the accompa-

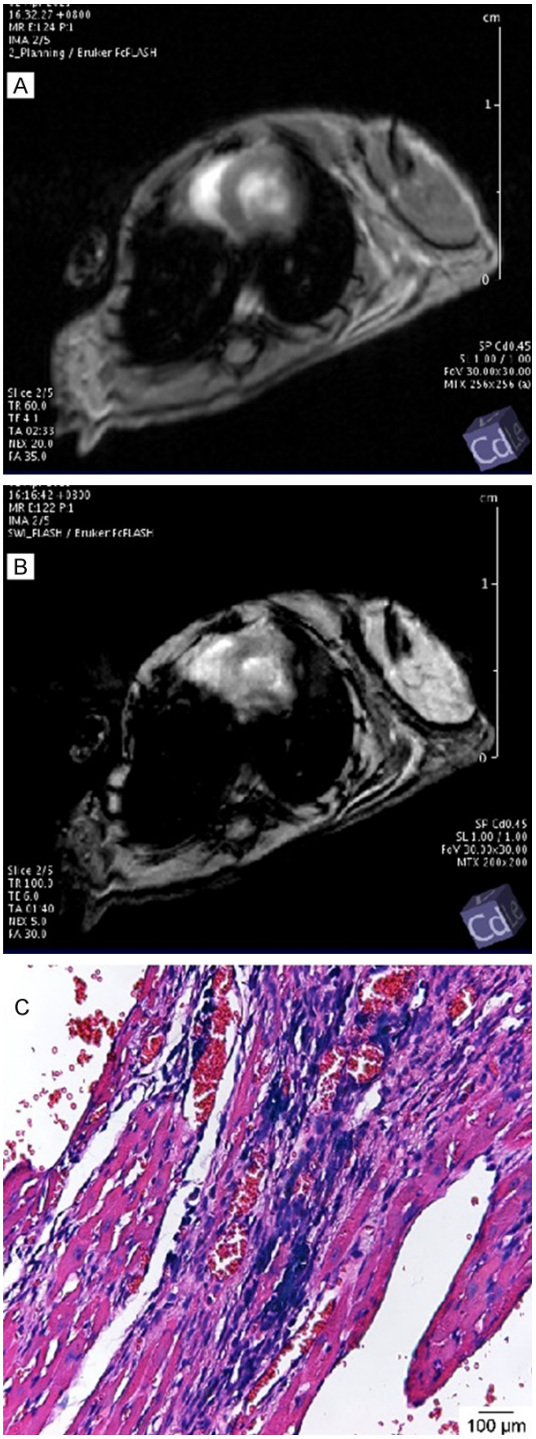

Figure 5. Cardiac MRI of Balb/c mice in the BMCS-treated group (A and B). Short-axis images with the GRE cine sequence on day 1 after myocardial injection of BMSC/LUC-USPIO. The signal of the anterior wall (white arrows) of the left ventricle was significantly decreased. Uneven delayed enhancement of the left ventricular septum can be observed on the right image. USPIO particle distribution (blue) in BMSCs in the myocardium of the chronic DIC mouse model (C).

nying fibrosis of chronic DIC is irreversible, multiple studies have demonstrated that mesenchymal stem cells can improve the outcomes of these patients. However, few studies have investigated the specific optimal number of MSCs for intramyocardial injection into lesions.

Since Balb/c mice are an inbred strain, we transplanted BMSCs derived from Balb/c mice into the myocardium of the same strain to avoid immune rejection. Therefore, this study reflects the real biological behaviors of BMSCs transplanted into the damaged hearts of a chronic DIC mouse model. The results showed that the signal of dual-labeled BMSCs derived from Balb/c mice and transplanted into DIC model mice (the same mouse strain) lasted less than 1 week, which is identical to the findings of our previous study [24].

As the study showed, even without immune rejection, the signals of transplanted BMSCs did not survive over 1 week, indicating that patches loaded with BMSCs or other beneficial biomaterials may be superior in improving the outcome of cardiovascular diseases characterized by the loss of myocardial fibers and cardiac fibrosis [31-33].

The significant differences between H9C2 cells treated with DOX and cultured in BMSC medium or normal DMEM imply that paracrine factors may be involved in improving the viability of BMSCs without inducing differentiation into myocytes. This finding indicates that extracellular vesicles derived from BMSCs could improve the outcomes of patients with chronic DIC, dilated cardiomyopathy and heart insufficiency.

We also found that the BLI trace signal lasted much longer than the MRI signal in chronic DIC mice, whereas MRI offered detailed pathophysiology data of chronic DIC. The MRI signal is visually undetectable at day 4 for all mouse intramyocardial injection of BMSC/LUC-USPIO. The T2* relaxome value measured by MRI was linearly correlated with the cell number, and a negative correlation between the number of cells and the T2 relaxome value was observed, which means we can infer the viable transplanted cell numbers by the T2* value not the T2 value. The optimal MRI parameters needed to obtain the best resolution of images were also identified in our current study.

In conclusion, BLI and MRI are ideal molecular imaging techniques to trace the biological behaviors of transplanted BMSCs in chronic DIC mice, and BLI is more sensitive. MRI could offer detailed message such as the location of transplanted BMSC/LUC-USPIO, and the lesion of chronic DIC.

Acknowledgements

This research was partially supported by the National Natural Science Foundation of China, 2019 (grant no. 81873891), the Major International (Regional) Joint Research Project of China, 2021 (grant no. 82020108018), China International Medical Foundation SKY Image Research Fund Project, 2019, Grant NO. Z-2014-07-1912-01 and the CAMS Innovation Fund for Medical Sciences (CIFMS), 2019 (grant no. 2019-I2M-1-001).

Disclosure of conflict of interest

None.

Address correspondence to: Dr. Yining Wang, Department of Radiology, State Key Laboratory of Complex Severe and Rare Diseases, Peking Union Medical College Hospital, Chinese Academy of Medical Sciences and Peking Union Medical College, 1 Shuaifuyuan, Beijing 100730, China. Tel: +86-13661003076; E-mail: wangyining@pumch.cn

References

[1] Kaiser J. A colorful chemotherapy agent could be made less toxic. Science 2020; 369: 18.

[2] Levis BE, Binkley PF and Shapiro CL. Cardiotoxic effects of anthracycline-based therapy: what is the evidence and what are the potential harms? Lancet Oncol 2017; 18: e445-e456.

[3] Curigliano G, Cardinale D, Dent S, Criscitiello C, Aseyev O, Lenihan D and Cipolla CM. Cardiotoxicity of anticancer treatments: epidemiology, detection, and management. CA Cancer J Clin 2016; 66: 309-325.

[4] Fradley MG. The evolving field of cardio-oncology: beyond anthracyclines and heart failure. Eur Heart J 2016; 37: 2740-2742.

[5] Zagar TM, Cardinale DM and Marks LB. Breast cancer therapy-associated cardiovascular disease. Nat Rev Clin Oncol 2016; 13: 172-184.

[6] Moslehi JJ. Cardiovascular toxic effects of targeted cancer therapies. N Engl J Med 2016; 375: 1457-1467.

[7] Armenian SH, Hudson MM, Mulder RL, Chen MH, Constine LS, Dwyer M, Nathan PC, Tissing WJ, Shankar S, Sieswerda E, Skinner R, Steinberger J, van Dalen EC, van der Pal H, Wallace WH, Levitt G and Kremer LC; International Late Effects of Childhood Cancer Guideline Harmonization Group. Recommendations for cardiomyopathy surveillance for survivors of childhood cancer: a report from the International Late Effects of Childhood Cancer Guideline Harmonization Group. Lancet Oncol 2015; 16: e123-e136.

[8] Getz KD, Sung L, Ky B, Gerbing RB, Leger KJ, Leahy AB, Sack L, Woods WG, Alonzo T, Gamis A and Aplenc R. Occurrence of treatment-related cardiotoxicity and its impact on outcomes among children treated in the AAML0531 clinical trial: a report from the Children's oncology Group. J Clin Oncol 2019; 37: 12-21.

[9] Yoshihara E, O'Connor C, Gasser E, Wei Z, Oh TG, Tseng TW, Wang D, Cayabyab F, Dai Y, Yu RT, Liddle C, Atkins AR, Downes M and Evans RM. Immune-evasive human islet-like organoids ameliorate diabetes. Nature 2020; 586: 606-611.

[10] Schweitzer JS, Song B, Herrington TM, Park TY, Lee N, Ko S, Jeon J, Cha Y, Kim K, Li Q, Henchcliffe C, Kaplitt M, Neff C, Rapalino O, Seo H, Lee IH, Kim J, Kim T, Petsko GA, Ritz J, Cohen BM, Kong SW, Leblanc P, Carter BS and Kim KS. Personalized iPSC-derived dopamine progenitor cells for Parkinson's disease. N Engl J Med 2020; 382: 1926-1932.

[11] Vazir A, Fox K, Westaby J, Evans MJ and Westaby S. Can we remove scar and fibrosis from adult human myocardium? Eur Heart J 2019; 40: 960-966.

[12] Bartunek J, Terzic A, Davison BA, Filippatos GS, Radovanovic S, Beleslin B, Merkely B, Musialek P, Wojakowski W, Andreka P, Horvath IG, Katz A, Dolatabadi D, El Nakadi B, Arandjelovic A, Edes I, Seferovic PM, Obradovic S, Vanderheyden M, Jagic N, Petrov I, Atar S, Halabi M, Gelev VL, Shochat MK, Kasprzak JD, Sanz-Ruiz R, Heyndrickx GR, Nyolczas N, Legrand V, Guédès A, Heyse A, Moccetti T, Fernandez-Aviles F, Jimenez-Quevedo P, Bayes-Genis A, Hernandez-Garcia JM, Ribichini F, Gruchala M, Waldman SA, Teerlink JR, Gersh BJ, Povsic TJ, Henry TD, Metra M, Hajjar RJ, Tendera M, Behfar A, Alexandre B, Seron A, Stough WG, Sherman W, Cotter G and Wijns W; CHART Program. Cardiopoietic cell therapy for advanced ischaemic heart failure: results at 39 weeks of the prospective, randomized, double blind, sham-controlled CHART-1 clinical trial. Eur Heart J 2017; 38: 648-660.

[13] Yau TM, Pagani FD, Mancini DM, Chang HL, Lala A, Woo YJ, Acker MA, Selzman CH, Soltesz

EG, Kern JA, Maltais S, Charbonneau E, Pan S, Marks ME, Moquete EG, O'Sullivan KL, Taddei-Peters WC, McGowan LK, Green C, Rose EA, Jeffries N, Parides MK, Weisel RD, Miller MA, Hung J, O'Gara PT, Moskowitz AJ, Gelijns AC, Bagiella E and Milano CA; Cardiothoracic Surgical Trials Network. Intramyocardial injection of mesenchymal precursor cells and successful temporary weaning from left ventricular assist device support in patients with advanced heart failure: a randomized clinical trial. JAMA 2019; 321: 1176-1186.

[14] Aminzadeh MA, Tseliou E, Sun B, Cheng K, Malliaras K, Makkar RR and Marbán E. Therapeutic efficacy of cardiosphere-derived cells in a transgenic mouse model of non-ischaemic dilated cardiomyopathy. Eur Heart J 2015; 36: 751-762.

[15] Armenian SH and Ehrhardt MJ. Optimizing cardiovascular care in children with acute myeloid leukemia to improve cancer-related outcomes. J Clin Oncol 2019; 37: 1-6.

[16] Singla DK, Johnson TA and Tavakoli Dargani Z. Exosome treatment enhances anti-inflammatory M2 macrophages and reduces inflammation-induced pyroptosis in doxorubicin-induced cardiomyopathy. Cells 2019; 8: 1224.

[17] Milano G, Biemmi V, Lazzarini E, Balbi C, Ciullo A, Bolis S, Ameri P, Di Silvestre D, Mauri P, Barile L and Vassalli G. Intravenous administration of cardiac progenitor cell-derived exosomes protects against doxorubicin/trastuzumab-induced cardiac toxicity. Cardiovasc Res 2020; 116: 383-392.

[18] Mousa HSE, Abdel Aal SM and Abbas NAT. Umbilical cord blood-mesenchymal stem cells and carvedilol reduce doxorubicin- induced cardiotoxicity: Possible role of insulin-like growth factor-1. Biomed Pharmacother 2018; 105: 1192-1204.

[19] Ezquer F, Gutiérrez J, Ezquer M, Caglevic C, Salgado HC and Calligaris SD. Mesenchymal stem cell therapy for doxorubicin cardiomyopathy: hopes and fears. Stem Cell Res Ther 2015; 6: 116.

[20] Singla DK. Akt-mTOR pathway inhibits apoptosis and fibrosis in doxorubicin-induced cardiotoxicity following embryonic stem cell transplantation. Cell Transplant 2015; 24: 1031-1042.

[21] Zhang Y, Yu Z, Jiang D, Liang X, Liao S, Zhang Z, Yue W, Li X, Chiu SM, Chai YH, Liang Y, Chow Y, Han S, Xu A, Tse HF and Lian Q. iPSC-MSCs with high intrinsic MIRO1 and sensitivity to TNF-α yield efficacious mitochondrial transfer to rescue anthracycline-induced cardiomyopathy. Stem Cell Reports 2016; 7: 749-763.

[22] De Angelis A, Piegari E, Cappetta D, Marino L, Filippelli A, Berrino L, Ferreira-Martins J, Zheng H, Hosoda T, Rota M, Urbanek K, Kajstura J, Leri A, Rossi F and Anversa P. Anthracycline cardiomyopathy is mediated by depletion of the cardiac stem cell pool and is rescued by restoration of progenitor cell function. Circulation 2010; 121: 276-292.

[23] Bellin M and Mummery CL. Stem cells: the cancer's gone, but did chemotherapy damage your heart? Nat Rev Cardiol 2016; 13: 383-384.

[24] Cao J, Li X, Chang N, Wang Y, Lei J, Zhao D, Gao K and Jin Z. Dual-modular molecular imaging to trace transplanted bone mesenchymal stromal cells in an acute myocardial infarction model. Cytotherapy 2015; 17: 1365-1373.

[25] Vagnozzi RJ, Maillet M, Sargent MA, Khalil H, Johansen AKZ, Schwanekamp JA, York AJ, Huang V, Nahrendorf M, Sadayappan S and Molkentin JD. An acute immune response underlies the benefit of cardiac stem cell therapy. Nature 2020; 577: 405-409.

[26] Huang H, Du X, He Z, Yan Z and Han W. Nanoparticles for stem cell tracking and the potential treatment of cardiovascular diseases. Front Cell Dev Biol 2021; 9: 662406.

[27] Guo B, Feng Z, Hu D, Xu S, Middha E, Pan Y, Liu C, Zheng H, Qian J, Sheng Z and Liu B. Precise deciphering of brain vasculatures and microscopic tumors with dual NIR-II fluorescence and photoacoustic imaging. Adv Mater 2019; 31: e1902504.

[28] Mitiouchkina T, Mishin AS, Somermeyer LG, Markina NM, Chepurnyh TV, Guglya EB, Karataeva TA, Palkina KA, Shakhova ES, Fakhranurova LI, Chekova SV, Tsarkova AS, Golubev YV, Negrebetsky VV, Dolgushin SA, Shalaev PV, Shlykov D, Melnik OA, Shipunova VO, Deyev SM, Bubyrev AI, Pushin AS, Choob VV, Dolgov SV, Kondrashov FA, Yampolsky IV and Sarkisyan KS. Plants with genetically encoded autoluminescence. Nat Biotechnol 2020; 38: 944-946.

[29] Iwano S, Sugiyama M, Hama H, Watakabe A, Hasegawa N, Kuchimaru T, Tanaka KZ, Takahashi M, Ishida Y, Hata J, Shimozono S, Namiki K, Fukano T, Kiyama M, Okano H, Kizaka-Kondoh S, McHugh TJ, Yamamori T, Hioki H, Maki S and Miyawaki A. Single-cell bioluminescence imaging of deep tissue in freely moving animals. Science 2018; 359: 935-939.

[30] Brusko TM, Russ HA and Stabler CL. Strategies for durable β cell replacement in type 1 diabetes. Science 2021; 373: 516-522.

[31] Huang S, Lei D, Yang Q, Yang Y, Jiang C, Shi H, Qian B, Long Q, Chen W, Chen Y, Zhu L, Yang W, Wang L, Hai W, Zhao Q, You Z and Ye X. A perfusable, multifunctional epicardial device improves cardiac function and tissue repair. Nat Med 2021; 27: 480-490.

[32] Montgomery M, Ahadian S, Davenport Huyer L, Lo Rito M, Civitarese RA, Vanderlaan RD, Wu J, Reis LA, Momen A, Akbari S, Pahnke A, Li RK, Caldarone CA and Radisic M. Flexible shape-memory scaffold for minimally invasive delivery of functional tissues. Nat Mater 2017; 16: 1038-1046.

[33] Stower H. Patching up hearts. Nat Med 2020; 26: 649.